LETTERS
PUBLISHED ONLINE: 25 SEPTEMBER 2011 | DOI: 10.1038/NMAT3119
nature materials

# A micromechanical model to predict the flow of soft particle glasses

Jyoti R. Seth[1], Lavanya Mohan[1], Clémentine Locatelli-Champagne[2], Michel Cloitre[2]* and Roger T. Bonnecaze[1]

**Soft particle glasses form a broad family of materials made of deformable particles, as diverse as microgels[1], emulsion droplets[2], star polymers[3], block copolymer micelles and proteins[4], which are jammed at volume fractions where they are in contact and interact via soft elastic repulsions. Despite a great variety of particle elasticity, soft glasses have many generic features in common. They behave like weak elastic solids at rest but flow very much like liquids above the yield stress. This unique feature is exploited to process high-performance coatings, solid inks, ceramic pastes, textured food and personal care products. Much of the understanding of these materials at volume fractions relevant in applications is empirical, and a theory connecting macroscopic flow behaviour to microstructure and particle properties remains a formidable challenge. Here we propose a micromechanical three-dimensional model that quantitatively predicts the nonlinear rheology of soft particle glasses. The shear stress and the normal stress differences depend on both the dynamic pair distribution function and the solvent-mediated EHD interactions among the deformed particles. The predictions, which have no adjustable parameters, are successfully validated with experiments on concentrated emulsions and polyelectrolyte microgel pastes, highlighting the universality of the flow properties of soft glasses. These results provide a framework for designing new soft additives with a desired rheological response.**

Soft particle glasses share common features with hard sphere glasses such as non-ergodicity and caged dynamics. However, whereas hard sphere colloids experience only forces due to excluded volume, soft particles at high volume fraction are compressed against each other by bulk osmotic forces and form flat facets at contact, with the average deformation depending on particle elasticity and volume fraction. The solvent forming the continuous phase is localized in thin films separating the particles (Supplementary Fig. S1). We model a soft particle glass as a suspension of $N$ non-Brownian, elastic spheres (Fig. 1a), which are dispersed at a volume fraction above the random close-packing of hard spheres ($\phi > \phi_c \approx 0.64$), in a solvent with viscosity $\eta_S$. The particles are slightly polydisperse in size, with an average radius $R$, which prevents them from crystallizing under flow. We characterize the contact between two particles by the overlap distance $h_{\alpha\beta}$ and the relative deformation $\varepsilon_{\alpha\beta} = h_{\alpha\beta}/R_c$, where $R_c$ is the contact radius (Fig. 1b). The suspension is subject to an imposed shear flow in the plane $(x, y)$ with shear rate $\dot{\gamma}$, particle and fluid inertia being neglected. As two compressed particles move past one another, a flow of solvent develops inside the liquid films separating the facets. This generates a net positive pressure, causing a further elastic deformation of the particles, which self-consistently maintains the lubricating films and makes particle motion possible. This mechanism shares strong similarities with the elastohydrodynamic (EHD) slippage of soft particles compressed against solid surfaces[5]. The interaction between $\alpha$ and $\beta$ is composed of a central repulsive force $\mathbf{f}^e_{\alpha\beta}$ associated with the elastic contact between the two particles, coupled to an EHD drag force $\mathbf{f}^{EHD}_{\alpha\beta}$, due to the motion of $\alpha$ relative to $\beta$.

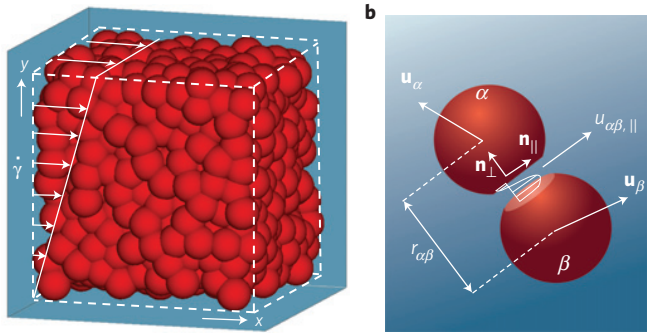


**Figure 1 | Structure and interactions of a model soft glass. a**, Typical configuration of jammed elastic spheres at $\phi = 0.8$; $\dot{\gamma}$ is the applied shear rate. **b**, Schematic showing pair-wise interactions between particles $\alpha$ and $\beta$ with radii $R_\alpha$ and $R_\beta$ centered at $\mathbf{x}_\alpha$ and $\mathbf{x}_\beta$ and translating with velocities $\mathbf{u}_\alpha$ and $\mathbf{u}_\beta$. $r_{\alpha\beta}$ is the centre-to-centre distance. $h_{\alpha\beta} = R_\alpha + R_\beta - r_{\alpha\beta}$ is the overlap distance; the thickness of the lubricating film separating the facets is much smaller that the overlap distance. The deformation of the particles is characterized by $\varepsilon_{\alpha\beta} = h_{\alpha\beta}/R_c$, where $R_c = R_\alpha R_\beta/(R_\alpha + R_\beta)$ is the contact radius. $u_{\alpha\beta,\parallel}$ is the component of the relative velocity parallel to the facets. The elastic force $\mathbf{f}^e_{\alpha\beta}$ and the EHD drag force $\mathbf{f}^{EHD}_{\alpha\beta}$ are parallel to the unit vectors normal ($\mathbf{n}_\perp$) and parallel ($\mathbf{n}_\parallel$) to the facets, respectively.

The elastic force $\mathbf{f}^e_{\alpha\beta}$ between soft particles such as elastomeric particles[6], microgels[7,8], and emulsion droplets[7] can be modelled using Hertzian-like potentials. The classical Hertz theory applies at rest and near equilibrium[6], where $\varepsilon_{\alpha\beta}$ less than 0.1. When the glass flows at high shear-rates, $\varepsilon_{\alpha\beta}$ can be much larger and Hertz theory underestimates the contact force. We used a modified approximate expression[6], which is valid up to $\varepsilon_{\alpha\beta} \approx 0.6$ : $\mathbf{f}^e_{\alpha\beta} = 4/3CE^*\varepsilon^n_{\alpha\beta}R_c^2\mathbf{n}_\perp$, where $E^* = E/2(1-\nu^2)$ is the contact modulus ($E$: Young modulus; $\nu = 0.5$: Poisson's ratio for incompressible spheres). The values of $n$ and $C$ vary with the degree of compression (Supplementary Fig. S2). It is interesting to note that the elastic energy associated with the elastic contact forces is generally much larger than $kT$ (Methods), indicating that the origin of the dynamics resides in the elastic properties of the particles themselves. The EHD drag

[1]Department of Chemical Engineering and Texas Materials Institute, The University of Texas at Austin, Austin, Texas 78712, USA, [2]Matière Molle et Chimie, UMR 7167 CNRS-ESPCI, Ecole Supérieure de Physique et Chimie Industrielles, 10 rue Vauquelin, 75005 Paris, France. *e-mail: michel.cloitre@espci.fr.

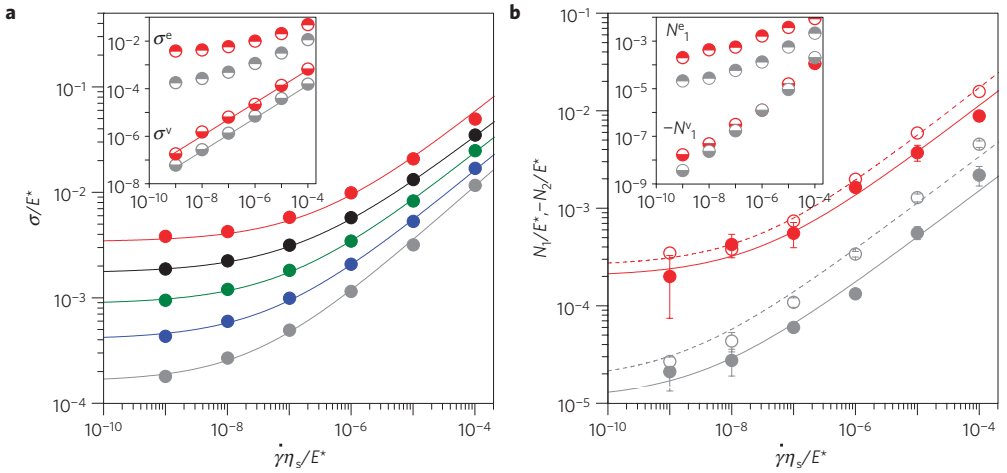


**Figure 2 | Computed shear stress and first and second normal stress differences of model soft glasses.** Each colour refers to a particular volume fraction: $\phi = 0.70$ (grey circle), $\phi = 0.75$ (blue circle), $\phi = 0.80$ (green circle), $\phi = 0.85$ (black circle), $\phi = 0.90$ (red circle). The shear stress and first normal stress differences data are denoted by full symbols, the second normal stress difference by open symbols. In **a**, the continuous lines represent the best fits to a Herschel–Bulkley equation (Supplementary Fig. S3); the inset shows the variations of the elastic and viscous components of the stress for $\phi = 0.70$ and $\phi = 0.90$; the full line has a slope 2/3. In **b**, we have plotted data only for $\phi = 0.70$ and $\phi = 0.90$ for the sake of clarity; the inset shows the variations of the elastic and viscous components of the first normal stress difference.

force $\mathbf{f}^{\mathrm{EHD}}_{\alpha\beta}$ is coupled to the repulsive elastic force $\mathbf{f}^{e}_{\alpha\beta}$ because the hydrodynamic pressure in the lubricating film supports the Hertzian pressure due to $\mathbf{f}^{e}_{\alpha\beta}$. We use the following expression based on the solution for a single particle dragged along a smooth surface[5,9]: $\mathbf{f}^{\mathrm{EHD}}_{\alpha\beta} = -(\eta_S C u_{\alpha\beta,\parallel} E^* R_c^3)^{1/2} \varepsilon^{(2n+1)/4}_{\alpha\beta} \mathbf{n}_{\parallel}$.

Both $\mathbf{f}^{e}_{\alpha\beta}$ and $\mathbf{f}^{\mathrm{EHD}}_{\alpha\beta}$ are assumed to be pairwise additive so that the net forces on particle $\alpha$, $\mathbf{F}^{e}_{\alpha}$ and $\mathbf{F}^{\mathrm{EHD}}_{\alpha}$, are the sum of the contributions from all facets. The motion is then described by the equation: $\mathbf{u}_\alpha = \mathrm{d}\mathbf{x}_\alpha/\mathrm{d}t = \mathbf{u}^{\infty}_{\alpha} + \mathrm{M}_\alpha[\mathbf{F}^{e}_{\alpha} + \mathbf{F}^{\mathrm{EHD}}_{\alpha}]$, where $\mathbf{u}^{\infty}_{\alpha}$ is the velocity field due to the applied shear rate, and $M_\alpha = f_r(\phi)/6\pi\eta_S R_\alpha$ is the mobility coefficient, which is that of a particle corrected by a factor $f_r(\phi)$ that accounts for its reduction at high volume fraction. The equation of motion is made dimensionless by scaling lengths, time and velocity by $R$, $\dot{\gamma}^{-1}$ and $\dot{\gamma}R$ respectively, so that

$$\frac{\mathrm{d}\tilde{\mathbf{x}}_\alpha}{\mathrm{d}\tilde{t}} = \tilde{\mathbf{u}}^{\infty}_{\alpha} + \frac{f_r(\phi)}{6\pi\tilde{R}_\alpha}\left[\frac{4}{3}C\tilde{\dot{\gamma}}^{-1}\sum_{\beta}\varepsilon^{n}_{\alpha\beta}\tilde{R}_c^2\mathbf{n}_{\perp} - \tilde{\dot{\gamma}}^{-1/2}\sum_{\beta}\left(C\tilde{u}_{\alpha\beta,\parallel}\tilde{R}_c^3\right)^{1/2}\varepsilon^{(2n+1)/4}_{\alpha\beta}\mathbf{n}_{\parallel}\right]$$

where the tilde quantities are dimensionless. The form of this equation shows that the dynamics is characterized solely by the dimensionless shear rate $\tilde{\dot{\gamma}} = \dot{\gamma}\eta_S/E^*$, which represents the ratio of viscous to elastic forces, and the overlap deformation $\varepsilon_{\alpha\beta}$, which depends on the volume fraction.

The $N$ coupled equations of motion were integrated numerically to determine the evolution of the spatial position and velocity of each particle, and the normalized steady-state shear stress $\sigma/E^*$ and first and second normal stress differences, $N_1/E^*$ and $N_2/E^*$, of the glass (see Methods). Figure 2a shows the simulated flow curves for five volume fractions between $\phi = 0.7$ and 0.9. The results are well described by the Herschel–Bulkley equation: $\sigma/E^* = \sigma_y/E^* + k_\sigma\tilde{\dot{\gamma}}^{m}$, with $m = 0.50 \pm 0.02$; $k_\sigma \propto G_0/E^*$, where $G_0$ is the low-frequency storage modulus, which has been determined independently[7]; $\sigma_y = G_0\gamma_y$ is the yield stress, where the yield strain $\gamma_y$ ranges from 0.02 to 0.04 (Supplementary Fig. S3). The shear thinning exponent $m = 1/2$ has been observed for soft particle suspensions very close to the jamming transition[10,11], in compressed emulsions[12], and in microgels[13]. Figure 2b shows the variations of the non-dimensional normal stress differences. They are roughly equal but opposite in magnitude ($N_2 \cong -2N_1$), indicative of a so-called film fluid[14]. At low shear rates they tend to a constant value whereas at high shear rates they grow proportionately to $\tilde{\dot{\gamma}}^{1/2}$. In the inset of Fig. 2a, we present the elastic component of the stress, $\sigma^e$, which arises from the distortion of particles during rearrangements and the viscous component, $\sigma^v$, due to the EHD drag force. The latter increases like $\sigma^v \propto \tilde{\dot{\gamma}}^{2/3}$, which differs from the variation $\sigma^v \propto \tilde{\dot{\gamma}}^{1/2}$ predicted for a 2d array of emulsion droplets[5,15]. Most importantly the magnitude of $\sigma^e$ is at least two orders of magnitude larger than $\sigma^v$. The inset of Fig. 2b shows similar results for normal stresses. The important result here is that the rheology of soft glasses is dominated by the elastic component of the stress associated with the alteration of the structure under flow.

The elastic stress $\sigma_e$ can be expressed in terms of the dynamic pair correlation function $g(\mathbf{r})$, which characterizes the distortion of the microstructure during shearing. Figure 3a shows azimuthal plots of $g(\mathbf{r})$ in the flow-gradient planes, which are indicative of the density of particle centres around a test particle of radius unity. During shear, neighbouring particles tend to accumulate in the upstream quadrant ($0 \le \theta \le \pi/2$), where they are more compressed, and deplete along the extensional axis ($\theta = 3\pi/4$), where they are less distorted. To relate these observations to the shear stress and normal stress variations, we have decomposed $g(\mathbf{r})$ into an orthogonal series of spherical harmonic functions[16,17] (see Supplementary Information). The coefficient $g_{2,-2}(r)$ of the expansion, which measures the asymmetry of the pair distribution between the compression and extension axes, is shown in Fig. 3b. The negative minimum at the radial distance $r_m$ is due to the accumulation of particles in the compressive region. The larger is the shear rate, the smaller $r_m$, indicating that particles are pushed closer. The depth of the minimum indicates more particles are on average in the compressive region; conversely the height of the maximum indicates fewer particles are on average in the extensional region. The elastic component of the shear stress can be computed from $g_{2,-2}(r)$ through[16]: $\sigma^e = -\rho^2\sqrt{\pi/15}\int_0^{2R} r^3 f^e(r) g_{2,-2}(r)\mathrm{d}r$, where $\rho$ is the average number density of particles and $f^e$ is the magnitude of the elastic force between two particles. The integral in the expression of $\sigma^e$ is dominated by the force at the point of maximum accumulation, where the particles are highly compressed. Thus, the stress can be accurately estimated by $\sigma \cong f_m\Sigma_m$, where $f_m$ is the

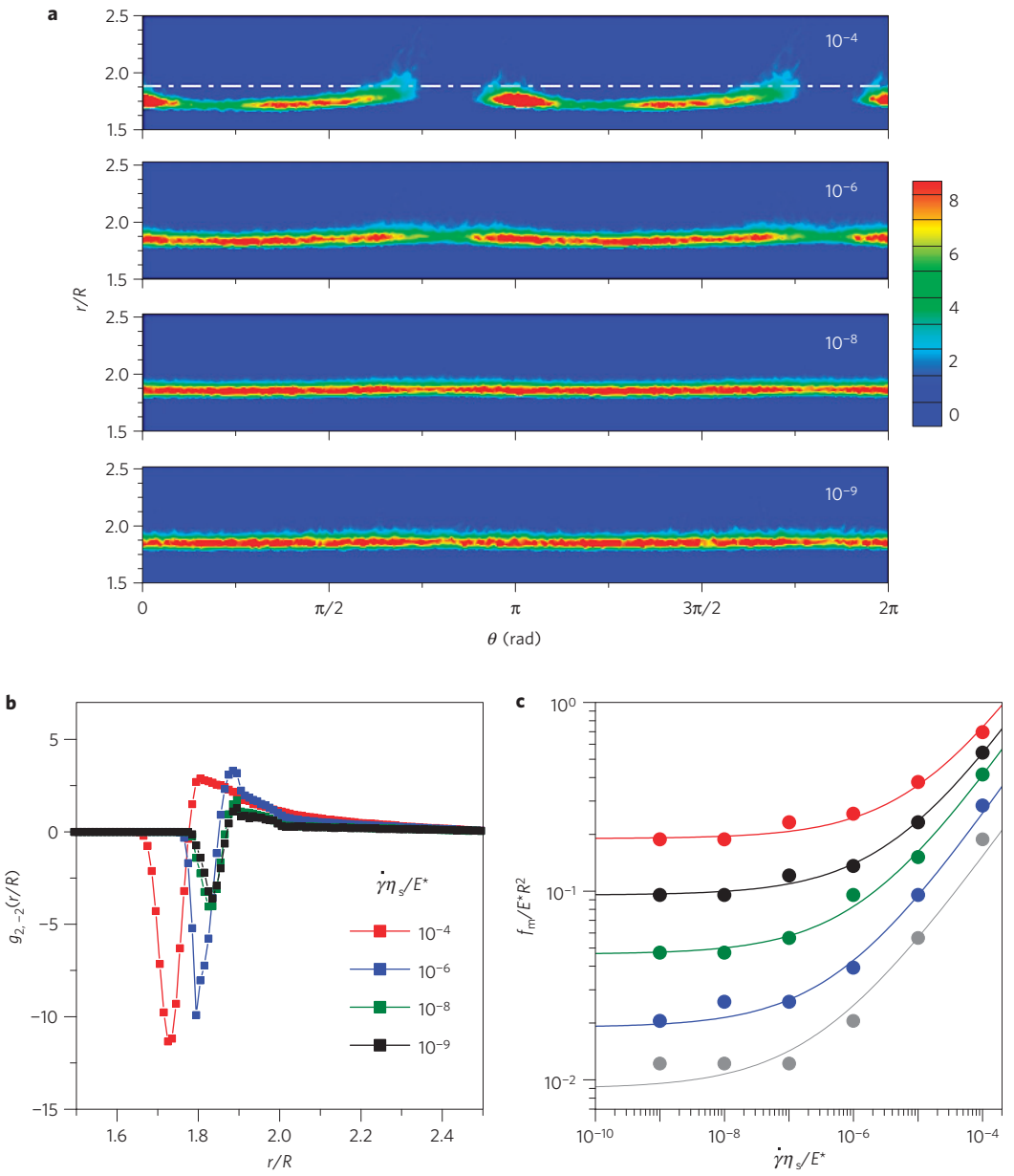


**Figure 3 | Microstructure of sheared soft particle glasses. a**, Azimuthal plots of the pair distribution function in the flow-gradient plane at different shear rates $\dot{\gamma}\eta_S/E^*$, which is indicative of the probability of finding a particle centre at position $(r, \theta)$ from a test particle centred at (0,0). Dark red colour indicates the highest probability of finding particle centres. The dashed line indicates the average centre-to-centre distance between particles at rest ($\phi = 0.80$). **b**, Spherical harmonic coefficients $g_{2,-2}(r)$ at different shear rates ($\phi = 0.80$). **c**, Dimensionless force at the radius of maximum accumulation versus applied shear rate for volume fractions studied in Fig. 2: $\phi = 0.70$ (grey circle), $\phi = 0.75$ (blue circle), $\phi = 0.80$ (green circle), $\phi = 0.85$ (black circle), $\phi = 0.90$ (red circle).

magnitude of the elastic force at $r = r_m$ and $\Sigma_m$ is the above integral of $g_{2,-2}(r)$ over the domain where $g_{2,-2}(r) < 0$. $\Sigma_m$ represents the surface density of contacts over a particle that significantly contributes to the stress. When the shear rate varies, $\Sigma_m$ is approximately constant (Supplementary Information), indicating that the contacts are redistributed but their surface density remains the same. The elastic force $f_m$ represents the force barrier that particles overcome to slide on top of one another. It is derived analytically using simple scaling arguments in the Supplementary Information: $\tilde{f}_m = \tilde{f}_y + k_f \dot{\tilde{\gamma}}^{1/2}$, where $\tilde{f}_{m(y)} = f_{m(y)}/E^*R^2$. The term in the right-hand side, $\tilde{f}_y \propto G_0/E^*$, represents the elastic force associated with a caged particle at the yield strain. The second term is an extra contribution due to the EHD deformation of the particles under flow; $k_f$ is a dimensionless coefficient that is proportional to the reduced low shear modulus $G_0/E^*$. To verify this prediction, $\tilde{f}_m$ was computed numerically from $r_m$ and the interparticle force law. Figure 3c shows the results for the five volume fractions investigated. The curves are well represented by a Herschel–Bulkley expression with a shear thinning exponent $m = 0.50 \pm 0.02$.

Using $\tilde{f}_m = \tilde{f}_y + k_f \dot{\tilde{\gamma}}^m$ and $\sigma_e \cong f_m \Sigma_m$, we then predict the following constitutive equation: $\sigma/\sigma_y = 1 + k(\dot{\gamma}\eta_S/\gamma_y^2 E^*)^{1/2}$, where $k$ is a numerical coefficient and $\gamma_y = \Sigma_m \tilde{f}_y R^2 (G_0/E^*)^{-1}$ is the yield strain. This result is successfully tested in Fig. 4a, which shows that the flow curves calculated for different volume fractions collapse onto a universal flow curve which is close to the prediction. The calculated yield strains also agree with the values determined directly from the simulated flow curves (see Supplementary Fig. S3). A similar analysis based on coefficients $g_{2,2}(r)$ and $g_{2,0}(r)$ of the expansion

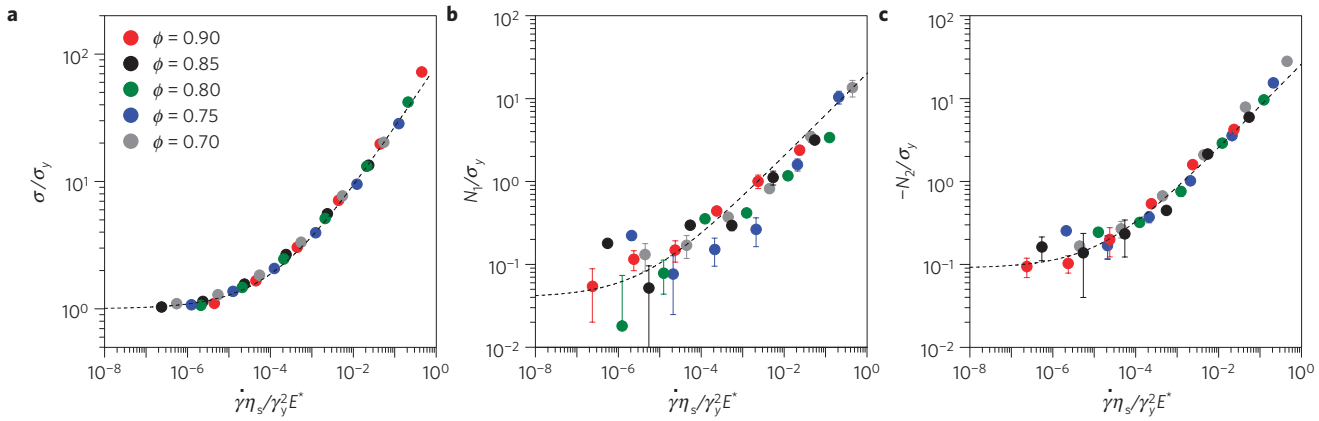


**Figure 4 | Universal constitutive laws for shear stress and normal stress differences from simulated data. a–c**, The dashed lines are the best fits to the constitutive equations derived in the text and Supplementary Section ($k = 80 \pm 3$; $k' = 20 \pm 2$; $k'' = 26 \pm 2$).

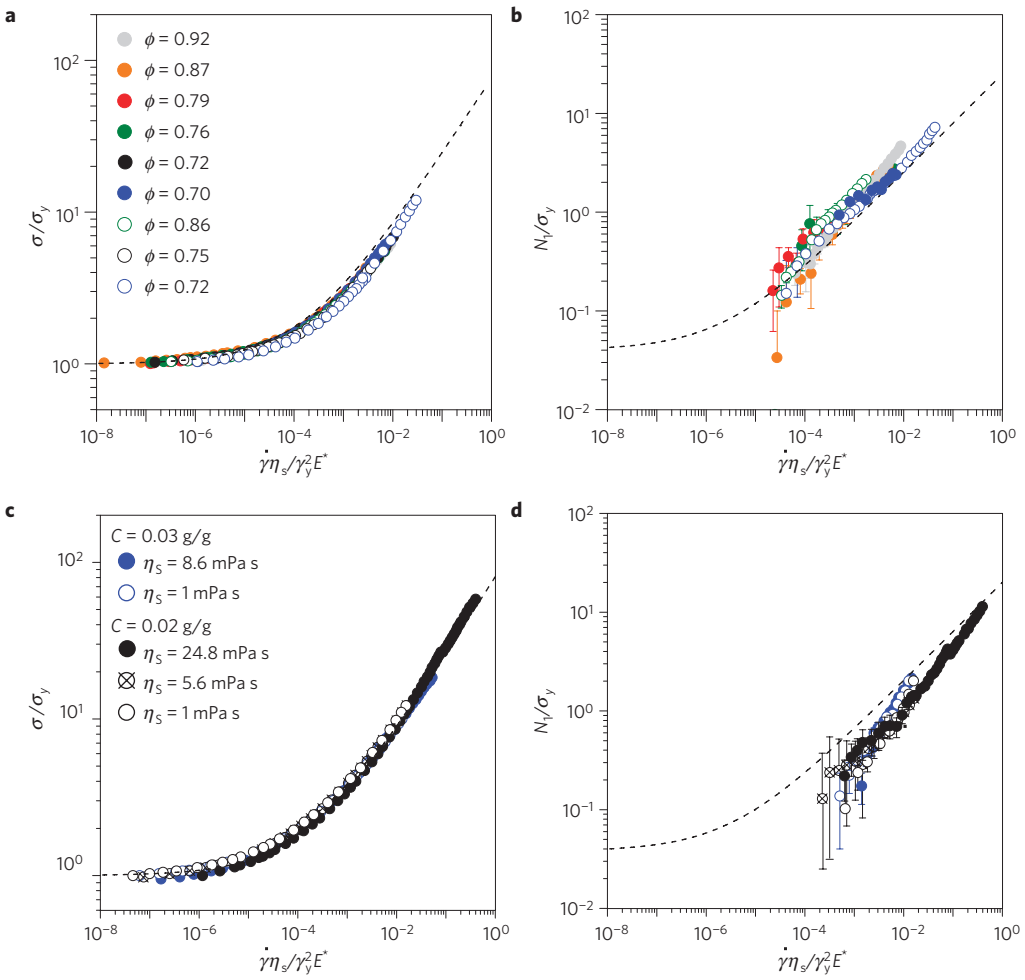


**Figure 5 | Universal scaling of shear stress and first normal stress difference experimental data. a,b**, Data for concentrated emulsions rescaled using $\sigma_y$, $\gamma_y$, and $E^*$ determined independently; solid symbols: oil in water–glycerol emulsions with $\eta_S = 7.9$ mPa s; open symbols: oil in water emulsions with $\eta_S$ = 1 mPa s. **c,d**, Data for microgel suspensions ($E^* = 40$ kPa). The dotted lines are the best fits to Herschel–Bulkley variations of the shear stress data and first normal stress differences obtained from the simulations. The raw data are presented in the Supplementary Figs S4 and S5.

(see Supplementary Information) yields similar relationships for the normal stress differences $N_1$ and $N_2$ (Fig. 4b-c).

To test these predictions we have studied the rheological properties of concentrated emulsions and suspensions of polyelectrolyte microgels with different volume fractions and solvent viscosities (see Methods). Measurements of the shear stress and first normal stress differences produce sets of data resembling those obtained from simulations (Supplementary Figs S4 and S5). The data for emulsions are rescaled in Fig. 5a,b using the values of $E^*$ and $\gamma_y$ determined experimentally. Both the shear stress and the normal stress differences collapse onto universal curves that are in good agreement with the theoretical predictions. For microgels, the

contact modulus is unknown and cannot be measured easily. To circumvent this difficulty, we determine $E^*$ in Fig. 5c by adjusting the experimental shear stress variations to the predicted flow curve. In Fig. 5d, we find that the resulting value also collapses the experimental first normal stress differences onto a universal curve that agrees with the prediction from the simulations. As an interesting application, we also deduce the effective shear modulus of individual microgels, $G_P \approx 20$ kPa, in qualitative agreement with independent estimates (Methods), and with values measured in macroscopic polyelectrolyte gels with similar composition[5,18].

The constitutive equations established here demonstrate the universality of the flow behaviour of soft glasses as a result of a subtle interplay between elastic interactions and structural rearrangements. This distinguishes our approach from other models of glassy dynamics which do not include contact forces and hydrodynamic contributions[19,20]. The importance of EHD lubrication between deformed particles is reflected by the key role played by the characteristic time $\eta_S/E^*$, which can be tuned by changing the viscosity of the continuous phase and/or the local elasticity through the particle architecture and composition. The alteration of the pair distribution function under flow together with the elastic contact forces accounts for the generic shear rate dependence of the shear and normal stress differences. At high shear rates, concentrated hard sphere suspensions also exhibit an accumulation and depletion of particle density along the compression and extension axes, but the stress is linearly proportional to the shear rate[21,22]. These results indicate that the soft particle glasses considered here form a class of materials singularly distinct from non-Brownian ideal hard sphere suspensions.

The theory and the experimental data we have presented are not very sensitive to the exact form of the interacting potential, so the generic properties reported here will be found in many other systems[23]. Our results open new strategies to estimate particle properties from macroscopic rheology and conversely provide rational tools for manufacturing and processing soft materials in industrial applications.

## Methods

**Simulation technique.** The model is implemented using a molecular dynamics-like simulation on random packings of $N$ elastic spheres confined in a cubic box that is periodically replicated. $N = 10^3$ in the simulations reported here, but the results with a much larger number of spheres ($N = 10^4$) were not significantly different. The radii of the spheres have a 10% polydispersity with an average radius of $R$, similar to that in the experimental systems examined later. We first created compressed random packings of force-free particles at the prescribed volume fraction $\phi$ following ref. 7. Constant shear rate simulations were then performed using the open source LAMMPS code[24] assuming Lees–Edwards boundary conditions. The position and the velocity of each particle were obtained by solving the $N$ equations of motion above using the Verlet integration algorithm[25]. The mobility coefficient correction factor $f_r(\phi)$ was equal to 0.01 for these simulations, but the results did not vary significantly for values of $f_r(\phi)$ less than 0.1. The viscous, elastic and total stress tensors were computed from the Kirkwood formula[26]: $\sigma^v = -\frac{1}{V}\sum_\beta^N \sum_{\alpha>\beta}^N \mathbf{f}_{\alpha\beta}^{EHD}(\mathbf{x}_\alpha - \mathbf{x}_\beta)$, $\sigma^e = -\frac{1}{V}\sum_\beta^N \sum_{\alpha>\beta}^N \mathbf{f}_{\alpha\beta}^{e}(\mathbf{x}_\alpha - \mathbf{x}_\beta)$, $\sigma = \sigma^v + \sigma^e$, where $V$ is the box volume. The shear stress $\sigma = \sigma_{yx}$, the first, and second normal stress differences, $N_1 = \sigma_{xx} - \sigma_{yy}$ and $N_2 = \sigma_{yy} - \sigma_{zz}$, respectively, were computed from the appropriate components of the stress tensor. These simulations were performed at non-dimensional shear rates $\tilde{\dot{\gamma}} = \dot{\gamma}\eta_s/E^*$ between $10^{-9}$ and $10^{-4}$. For every $(\tilde{\dot{\gamma}}, \phi)$ combination, $\sigma$, $N_1$ and $N_2$ were calculated at regular time intervals until steady state was reached. Steady-state values were then determined by averaging over several strain units. The results reported in this paper were obtained by averaging over five runs with different initial configurations of particles for each volume fraction and shear rate.

**Preparation of emulsions.** The emulsions are dispersions of silicone oil (viscosity: 0.5 mPa s) in aqueous solvents stabilized by the non-ionic surfactant Triton X. They were prepared according to the well established protocol previously described[5]. To ensure purely repulsive interactions, the emulsions were washed after preparation to eliminate the excess surfactant and avoid depletion interactions between droplets. The droplet size distribution and the structure of the emulsions were determined from confocal microscopy observations. The mean particle radius is $R \approx 1.25\,\mu$m with a polydispersity of about 20%. The structure of the emulsions remains disordered at all volume fractions. The contact elastic modulus $E^*$ was determined from the radius $R$ and the interfacial tension $\gamma_i$ using the relation[7]: $E^* = 9.92\,\gamma_i/R$. The latter was measured using the pendant drop method. The solvents are water ($\eta_S = 1$ mPa s, $\gamma_i \approx 5$ mJ m$^{-2}$, $E^* \approx 40$ kPa) and a water–glycerol mixture ($\eta_S = 7.9$ mPa s, $\gamma_i \approx 4$mJ m$^{-2}$, $E^* \approx 32$ kPa). The volume fraction was set by centrifugation and was measured both by gravimetry and by image processing. With these values of $R$ and $E^*$ and $\varepsilon = 0.1$, the ratio $E^*\varepsilon^{5/2}R^3/kT$ is much larger than 1 ($\approx 10^5$).

**Preparation of microgels.** We used polyelectrolyte microgels consisting of a cross-linked copolymer network of ethyl acrylate and methacrylic acid. The microgels are collapsed at low pH and swell when there are ionized by NaOH. At low concentrations, the collapsed and swollen microgels are spherical particles with a hydrodynamic radius $R = 50$ nm and $R = 230$ nm, respectively. They form glasses above close-packing. The particles tend to shrink when the concentration is increased so that the actual volume fraction cannot be determined accurately[27]. We used the polymer concentration $C$ as the control parameter. At swelling equilibrium, the shear modulus of the particle, $G_P$, and the osmotic pressure of the counterions inside the particles are expected to be equal[28], which provides an order of magnitude[27] of $G_P \approx 50$ kPa. With the values of $E^*$ and $R$ for microgels and $\varepsilon = 0.1$, the ratio $E^*\varepsilon^{5/2}R^3/kT$ is also much larger than 1 ($\approx 10^3$).

**Rheological measurements.** Measurements are made using an Anton-Paar MCR 501 rheometer mounted with a cone and Peltier plate geometry and a solvent trap (diameter: 50 mm; angle: 2°; truncation: 48 μm; temperature: 20 °C). The shearing surfaces are coated with waterproof sandpaper, providing a surface roughness of 20 μm which prevents the occurrence of slip[5].

Received 12 July 2010; accepted 15 August 2011; published online 25 September 2011

## References


1. Mattsson, J. *et al.* Soft colloids make strong glasses. *Nature* **462,** 83–86 (2009).
2. Mason, T. G., Bibette, J. & Weitz, D. A. Elasticity of compressed emulsions. *Phys. Rev. Lett.* **75,** 2051–2054 (1995).
3. Mayer, C. *et al.* Asymmetric caging in soft colloidal mixtures. *Nature Mater.* **7,** 780–784 (2008).
4. Zhoua, E. H. *et al.* Universal behavior of the osmotically compressed cell and its analogy to the colloidal glass transition. *Proc. Natl Acad. Sci. USA* **106,** 10632–10637 (2009).
5. Meeker, S. P., Bonnecaze, R. T. & Cloitre, M. Slip and flow in soft particle pastes. *Phys. Rev. Lett.* **92,** 198302 (2004).
6. Liu, K. K., Williams, D. R. & Briscoe, B. J. The large deformation of a single micro-elastomeric sphere. *J. Phys. D.* **31,** 294–303 (1998).
7. Seth, J., Cloitre, M. & Bonnecaze, R. T. Elastic properties of soft particle pastes. *J. Rheol.* **50,** 353–376 (2006).
8. Zhang, Z. *et al.* Thermal vestige of the zero-temperature jamming transition. *Nature* **459,** 230–233 (2009).
9. Seth, J. R. *On the Rheology of Dense Pastes of Soft Particle* PhD thesis, Univ. Texas (2008).
10. Tighe, B. P., Wodhuis, E., Remmers, J. J. C., van Saarloos, W. & van Hecke, M. Model for the scaling of stresses and fluctuations in flows near jamming. *Phys. Rev. Lett.* **105,** 088303 (2010).
11. Nordstrom, K. N. *et al.* Microfluidic rheology of soft colloids above and below jamming. *Phys. Rev. Lett.* **105,** 175701 (2010).
12. Princen, H. M. & Kiss, A. D. Rheology of foams and highly concentrated emulsions: IV. An experimental study of the shear viscosity and yield stress of concentrated emulsions. *J. Colloid Interface Sci.* **128,** 176–187 (1989).
13. Cloitre, M., Borrega, R., Monti, F. & Leibler, L. Glassy dynamics and flow properties of soft colloidal pastes. *Phys. Rev. Lett.* **90,** 068303 (2003).
14. Larson, R. G. The elastic stress in film fluids. *J. Rheol.* **41,** 365–372 (1997).
15. Denkov, N. D., Tcholakova, S., Golemanov, K., Ananthapadmanabhan, K. P. & Lips, A. Viscous friction in foams and concentrated emulsions under steady shear. *Phys. Rev. Lett.* **100,** 138301 (2008).
16. Hanley, H. J. M., Rainwater, J. C. & Hess, S. Shear-induced dependence of the liquid pair correlation function. *Phys. Rev. A* **36,** 1795–1802 (1987).
17. Morris, J. F. & Katyal, B. Microstructure from simulated Brownian suspension flows at large shear rate. *Phys. Fluids* **14,** 1920–1937 (2002).
18. Schosseler, F., Ilmain, F. & Candau, S. J. Structure and properties of partially neutralized poly (acry1ic acid) gels. *Macromolecules* **24,** 225–234 (1991).
19. Sollich, P., Lequeux, F., Hébraud, P. & Cates, M. E. Rheology of soft glassy materials. *Phys. Rev. Lett.* **78,** 2020–2023 (1997).
20. Fuchs, M. & Cates, M. E. Theory of nonlinear rheology and yielding of dense colloidal suspensions. *Phys. Rev. Lett.* **89,** 248304 (2002).
21. Brady, J. H. & Morris, J. F. Microstructure of strongly sheared suspensions and its impact on rheology and diffusion. *J. Fluid Mech.* **348,** 103–139 (1997).
22. Crassous, J. J. *et al.* Shear stresses of colloidal dispersions at the glass transition in equilibrium and in flow. *J. Chem. Phys.* **128,** 204902 (2008).
23. Erwin, B., Vlassopoulos, D., Gauthier, M. & Cloitre, M. Dynamics and rheology of colloidal star polymers. *Soft Matter* **6,** 2825–2833 (2010).

24. Plimpton, S. J. Fast parallel algorithms for short-range molecular dynamics. *Comput. Phys.* **117,** 1–19 (1995).
25. Rapaport, D. C. *The Art of Molecular Dynamics Simulation* (Cambridge Univ. Press, 2004).
26. Larson, R. G. *The Structure and Rheology of Complex Fluids* (Oxford Univ. Press, 1999).
27. Borrega, R., Cloitre, M., Betremieux, I., Ernst, B. & Leibler, L. Concentration dependence of the low-shear viscosity of polyelectrolyte micro-networks: From hard spheres to soft microgels. *Europhys. Lett.* **47,** 729–735 (1999).
28. Rubinstein, M., Colby, R. H. & Dobrynin, A. V. Elastic modulus and equilibrium swelling of polyelectrolyte gels. *Macromolecules* **29,** 398–406 (1996).

## Acknowledgements

We are grateful to D. Vlassopoulos for a critical reading of the manuscript. This work was supported by the NoE European Network Sofcomp, the CNRS (PICS 4176), the Petroleum Research Fund (ACS PRF #41236-AC9), and the National Science Foundation (CBET 0854420).

## Author contributions

J.R.S, L.M. and R.T.B. conceived the model, developed the simulations and analysed the results. C.L. and M.C. conceived and conducted the experiments and analysed the results. M.C. and R.T.B. interpreted and synthesized the results and wrote the paper. J.R.S., L.M. and C.L. provided editorial comments on the paper.

## Additional information

The authors declare no competing financial interests. Supplementary information accompanies this paper on www.nature.com/naturematerials. Reprints and permissions information is available online at http://www.nature.com/reprints. Correspondence and requests for materials should be addressed to M.C.